IEEE Access
Multidisciplinary | Rapid Review | Open Access Journal

Date of publication xxxx 00, 0000, date of current version xxxx 00, 0000.

Digital Object Identifier 10.1109/ACCESS.2017.Doi Number

IoT and biosensors: a smart portable potentiostat with advanced cloud-enabled features

Valentina Bianchi[1], Senior Member, IEEE, Andrea Boni[1], Member, IEEE, Marco Bassoli[1], Marco Giannetto[2], Simone Fortunati[2], Maria Careri[2] and Ilaria De Munari[1], Senior Member, IEEE

[1]Department of Engineering and Architecture, University of Parma, 43124 Parma, Italy
[2]Department of Chemistry, Life Sciences and Environmental Sustainability, University of Parma, 43124 Parma, Italy

Corresponding author: Andrea Boni (e-mail: andrea.boni@unipr.it).

This work was supported by the project "Biosensoristica innovativa per i test sierologici e molecolari e nuovi dispositivi PoCT per la diagnosi di infezione da SARS-CoV-2" funded in 2020 by "Bando Straordinario di Ateneo per Progetti di Ricerca Biomedica in Ambito SARS-COV-2 e COVID-19" – University of Parma

ABSTRACT Recent advances in Internet-of-Things technology have opened the doors to new scenarios for biosensor applications. Flexibility, portability, and remote control and access are of utmost importance to move these devices to people's homes or in a Point-of-Care context and rapidly share the results with users and their physicians. In this paper, an innovative portable device for both quantitative and semi-quantitative electrochemical analysis is presented. This device can operate autonomously without the need of relying on other devices (e.g., PC, tablets, or smartphones) thanks to built-in Wi-Fi connectivity. The developed hardware is integrated into a cloud-based platform, exploiting the cloud computational power to perform innovative algorithms for calibration (e.g., Machine Learning tools). Results and configurations can be accessed through a web page without the installation of dedicated APPs or software. The electrical input/output characteristic was measured with a dummy cell as a load, achieving excellent linearity. Furthermore, the device response to five different concentrations of potassium ferri/ferrocyanide redox probe was compared with a bench-top laboratory instrument. No difference in analytical sensitivity was found. Also, some examples of application-specific tests were set up to demonstrate the use in real-case scenarios. In addition, Support Vector Machine algorithm was applied to semi-quantitative analyses to classify the input samples into four classes, achieving an average accuracy of 98.23%. Finally, COVID-19 related tests are presented and discussed.

INDEX TERMS Amperometric Sensors, Biosensors, Current Measurement, Remote Monitoring, Health Monitoring, Cloud Services, IoT Sensors, Machine Learning Application.

I. INTRODUCTION

The recent development of Information and Communications Technologies (ICT), designed for the Internet of Things (IoT) framework, has led to an increased interest in the study of new smart, portable, and interconnected devices in different application fields [1], [2]. Electrochemical analyses and, in particular, biosensing applications are not an exception [3]–[5]. Traditionally, the identification of clinically relevant biomarkers for disease diagnosis and follow-up is carried out with bench-top instrumentation (i.e., potentiostats) in a dedicated laboratory [6], [7]. With the advent of IoT technologies, it is possible to design new portable potentiostats that open the doors to innovative features. The possibility of moving these devices to different locations will bring the laboratory closer to people's homes, according to a Point-of-Care (PoC) context, allowing periodic analyses more easily (e.g. follow-up of a particular pathology) or the immediate sharing of the results with the physicians [8].

For example, in the recent COVID-19 pandemic scenario, the implementation of rapid and delocalized serological or salivary/swab tests for the quantification of specific antibodies (i.e anti-nucleocapsid and/or anti-spike related to SARS-CoV-2) or viral antigen (spike protein) would certainly have improved and aided the contact tracing management.

The developed hardware should be adequate for both quantitative and semi-quantitative measurements making the

This article has been accepted for publication in a future issue of this journal, but has not been fully edited. Content may change prior to final publication. Citation information: DOI 10.1109/ACCESS.2021.3120022, IEEE Access

device suitable for general purposes. Moreover, regardless of the particular kind of analysis, device calibration is often necessary: for semi-quantitative tests, a threshold should be set to discriminate different classes of samples (e.g., positives or negatives) [9]; conversely, for quantitative analyses, a calibration function should be assessed to measure the concentration of the analyte in the sample under test [10]. In this regard, a solution could be the development of edge solutions. Research toward IoT edge devices is moving fast [11]. However, the possibility of remotely reconfiguring the device in a simple and intuitive way, is mandatory in some application domains. For example, the calibration process could be carried out once in a laboratory environment with the resulting parameters stored in a repository located in a cloud service. The portable device can be properly configured before a testing campaign by downloading the suitable parameters, according to a given PoC analysis. It is worth to be noted that if different analyses have to be performed with the same hardware device, the smart potentiostat can easily reconfigure itself by downloading a different set of calibration parameters from the cloud. To implement these features, the device must be connected to the Internet without relying on other devices such as a smartphone.

Another important aspect is the possibility to perform analyses also in locations not covered by an Internet connection. Then, the device should have a suitable data processing capability to elaborate the acquired data on-board and send the results to the cloud when the link is restored. Signal elaboration at the edge limits the amount of data transferred and the activation the power-hungry radio interface, leading to lower energy consumption in some applications.

This paper presents a smart, portable, and cloud-based reconfigurable potentiostat for both semi-quantitative and quantitative analyses. The idea is to design a device for different types of analyses with an easy-to-use web-based interface to simplify the configuration process, easily accessible from any PCs, tablets, or smartphones, without the need for a custom, application-specific software. This feature allows either PoC or home use, even by people with no or poor technical skills. The calibration process exploits an analytics platform based on a cloud service used to store the evaluated parameters for subsequent download. Moreover, the computing capacity of the cloud service enables the use of advanced techniques such as Machine Learning (ML) to improve the classification accuracy of the test results. The MATLAB Thingspeak platform for IoT [13] was used in the proposed implementation since it enables cloud-based data processing with MATLAB routines. Therefore, built-in Machine Learning MATLAB functions are exploited to demonstrate the advantage of combining cloud-based services with smart portable potentiostats.

To build a historical record of the analysis results for each person and help to share data with physicians (e.g. in the case of multiple patients using the same device), an automatic association procedure between the user and his/her measurements was added.

The proposed hardware was designed to achieve comparable performance to bench-top instruments for quantitative and semi-quantitative analyses. In addition, since the device is conceived to work also without any network link, the on-board data acquisitions processing was considered of primary importance.

The paper is organized as follows: in section II, related works are discussed; in section III, the system architecture is depicted and both hardware and web components are detailed; in section IV, tests are described and the experimental results are presented and discussed. Finally, in section V, conclusions are drawn.

II. RELATED WORKS

In general, three main sections can be highlighted in all the portable potentiostats already developed and described in the literature: hardware, firmware, and connectivity units. A schematic example is shown in Fig. 1. The proposed approaches differ from each other according to the solutions adopted for each unit.

The hardware section of the potentiostat is interfaced with the amperometric sensor based on a three-electrode electrochemical cell consisting of a working electrode (WE), a counter electrode (CE), and a reference electrode (RE). The simplified electrical model is shown in Fig. 2, where R_S is the solution resistance between CE and RE pins, R_{CH} and C_{CH} represent the faradaic resistance and the double-layer capacitance at the WE pin, and I_C models the charge generated by the electron transfer associated to the faradic reaction occurring in the sensor cell [12]. The faradaic resistance and the capacitance at the CE pin are not included in the model

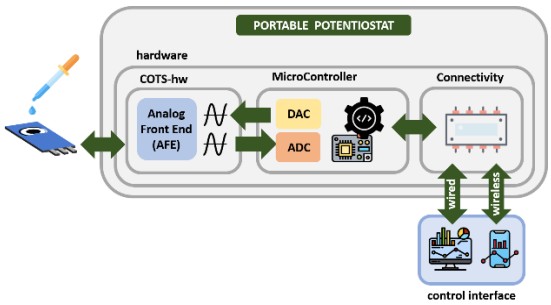

FIGURE 1. Typical architecture of a portable potentiostat.

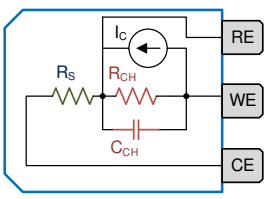

FIGURE 2. Simplified equivalent circuit of an electrochemical cell.

This article has been accepted for publication in a future issue of this journal, but has not been fully edited. Content may change prior to final publication. Citation information: DOI 10.1109/ACCESS.2021.3120022, IEEE Access

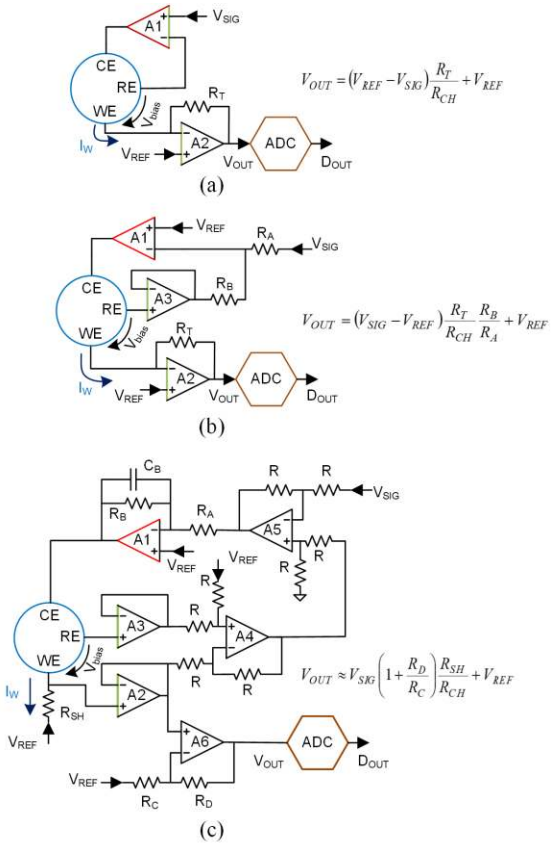

FIGURE 3. Potentiostats COTS hardware architectures.

since they are usually negligible. The hardware unit sets the bias voltage of the cell and senses the current flowing from the WE pin. The bias voltage V_{bias}, corresponding to the voltage difference between the WE and the RE terminals, is controlled with a feedback circuit driving the CE pin. When a suitable V_{bias} input is applied to the cell, a chemical reaction is induced. The output current (flowing from/into the WE pin) is related to the concentration of the target analyte and cell bias voltage.

Focusing on Components-Off-The-Shelf (COTS) implementations, some hardware architectures are proposed in the literature (Fig. 2). The circuit in Fig. 2(a) is a Single-Ended Potentiostat (SEP) with two opamps (SEP-2) [13]–[15]. This implementation exhibits the minimum component count and power consumption. Therefore, it is the best candidate for portable devices. A critical device is the control opamp A1 that must exhibit a very low input current to not perturb the voltage at the RE pin and a low output resistance to drive the equivalent capacitance C_{CH}, which can be in the microfarad range in the sensor model in Fig. 2. A further relevant specification of this opamp is the maximum output current, setting the time required for the initial conditioning of the cell [16]. In the triple-opamp configuration (SEP-3) in Fig. 2(b), the voltage at the CE pin is controlled with a circuit involving two opamps in the loop (i.e. A1 and A3) [12], [17], [18]. This solution allows the requirements on amplifier A1 in the SEP-2 implementation to be split over two different opamps. Indeed, only the amplifier connected to the RE pin (i.e. A3) must exhibit a low input current, whereas a suitable driving capability is required to A1. The drawback is the larger component count and power consumption.

In SEP-2 and SEP-3 circuits, a TransImpedance Amplifier (TIA) is required to sense the cell current and set the WE voltage. The input impedance $Z_{IN\text{-}TIA}$ of this amplifier is a critical aspect of those architectures since it affects the stability margins of the control amplifier A1. Indeed, $Z_{IN\text{-}TIA}$ is a part of the feedback network of A1 with the equivalent impedance network in the electrical model of the amperometric cell, Fig. 2. Even though this issue is relevant and may lead to instability [19], it is often overlooked in COTS-based potentiostat implementation.

Another issue of these circuits is the sensitivity to the crosstalk noise due to electrical coupling to the WE pin. Indeed, the TIA input impedance exhibits relevant positive reactance (i.e., inductive behavior) from a frequency value depending on the unity-gain frequency (GBW) of A2 and the feedback resistor R_T. Thus, the potentiostat is expected to have a significant sensitivity to any electrical signal coupled to WE in this frequency band and, for this reason, the shielding of the wire and Printed Circuit Board (PCB) trace connecting WE to the TIA input should be carefully considered [20].

The circuit in Fig. 2(c) is a Differential Architecture (DA) for COTS implementation [21]. The bias voltage of the cell is directly controlled through a feedback loop involving two differential amplifiers (based on opamps A4 and A5) and a Proportional-Integral (PI) controller. The latter block is implemented with an active low-pass filter based on opamp A1 with the feedback network including R_A, R_B, and C_B.

It is worth noting that in the solution of Fig. 2(c) the voltage at the WE pin cannot be independently set by a TIA. Therefore, a low-value shunt resistance (R_{SH}) is introduced to sense the cell current. Thus, this configuration provides a low broadband impedance at the WE pin with benefits in terms of sensitivity to coupled noise and disturbance. Furthermore, a PI controller in the loop ensures a suitable stability margin over a large concentration range with different chemical species and substrate materials. However, the main disadvantage of this implementation is the large component count and, consequently, the largest power consumption.

In all the solutions presented in Fig. 2, the interface between the hardware and the firmware section is represented by the Analog-to-Digital-Converter (ADC). If the three circuits are compared in terms of Root Mean Square (RMS) noise voltage at the ADC input, the worst performance is achieved by the DA implementation due to the largest number of opamps in the controlling loop, each contributing with its own input-referred noise voltage. Furthermore, the SEP-3 is expected to exhibit a larger noise voltage than the SEP-2, since two opamps are in the CE control loop instead of one.

The choice of the ADC used, together with that of the DAC exploited to generate the cell conditioning signals (i.e., V_{sig} and V_{ref}), has a considerable impact on the measurement

This article has been accepted for publication in a future issue of this journal, but has not been fully edited. Content may change prior to final publication. Citation information: DOI 10.1109/ACCESS.2021.3120022, IEEE Access

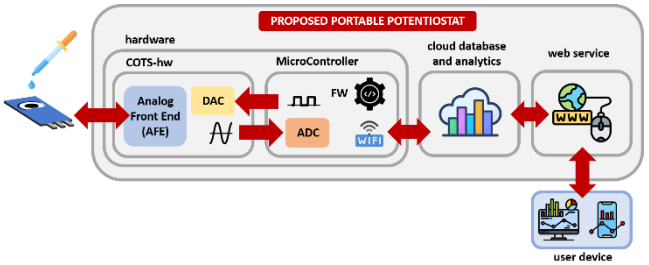

FIGURE 4. Proposed system architecture.

accuracy. Exploiting the ADC and DAC, embedded in the MicroController Unit (MCU), usually results in a lower resolution (e.g. 12 bits ADC/DAC [18], [22]) in respect to using a dedicated component (e.g. 20bits [23]). However, this solution is usually preferred in portable devices since it reduces costs and the number of the involved components.

Other important aspects of a portable potentiostat are the communication protocol to maximize portability, the control interface, and the reliance on different devices for the operations. All these choices imply the proper design of the microcontroller processing and connectivity sections of Fig. 1. Some solutions recently proposed by Adams et al. [18], [24], even if very compact and embedding promising hardware, require a USB connection to transfer data and a PC to control the instrument, thus limiting the device portability. Bluetooth technology is a solution shared among different devices proposed in the literature [22], [25], [26] to enhance portability. Due to the low transmission range of the Bluetooth technology, these solutions rely on a smartphone for control and data recording. Different control APPs were developed based on different operating system (OS) versions. Wi-Fi connectivity is exploited in [27]. This solution allows sharing data without the need for an external device. However, a desktop power supply is adopted, thus effectively preventing the device portability. In [28], a Wi-Fi potentiostat based on LMP91000 hardware, which allows only semi-quantitative analyses, is presented. In [15], [29], a Wi-Fi solution used to transfer analyses results to the cloud is proposed. In this case, the developed hardware exhibits a limited versatility since the reading range is fixed, i.e. from -210µA to 70µA, even if it is capable of quantitative analyses with high accuracy. Device configuration is embedded into the device firmware, and the cloud service is exploited only for data visualization and sharing. A first and very preliminary improvement with a programmable reading range is presented in [30].

III. MATERIALS AND METHODS

The proposed potentiostat is shown in Fig. 4. Differently from the implementations reported in the literature, the device architecture also includes cloud services (i.e. analytics and database), with a web service acting as the interface between the cloud and the user devices (e.g. PC, tablet, smartphone). In particular, cloud analytics is in charge of evaluating the parameters of the calibration function, which are stored in the cloud database together with the user ID and the corresponding analysis results.

The calibration function relies on a prediction model to assess the unknown concentrations of analytes of interest from the device output. Such a model is obtained from a preliminary calibration of the device with reference standards at known concentrations. Different calibration functions can be used depending on the analysis to be performed. The transfer of the parameter calculations on an analytic platform allows calibration to be performed once, thus enabling easy reconfiguration of the device based on the target analysis and, consequently, on the parameters of the selected calibration function. As a result, the required configuration can be chosen among those available online, allowing the device to perform different tests without the need for recalibration at each configuration change.

The analyte concentration measurements are performed locally on-board (hardware section in Fig. 4). During this process, the device first downloads the parameters from the Internet through the Wi-Fi connection and then, after data processing, uploads the result to the cloud for storage and remote retrieval. The parameters download phase is required only once at the beginning of the measurement and the Wi-Fi connection is no longer required until a result is uploaded. However, if the connectivity is lost during the upload, the device can store the results in the internal memory and send them to the cloud later. This feature increases the device's versatility, which retains its full functionalities even in the absence of any Wi-Fi networks.

Moreover, exploiting the computing capability of a cloud service for calibration allows the implementation of complex functions and improves the whole system features. For example, Machine Learning Classification Algorithms can be implemented to train the system to discriminate the samples among different classes (e.g. positives or negatives).

The system core is an MCU based on ARM Cortex-M4 with built-in support for Wi-Fi protocol (CC3200 [31]). Dedicated hardware was designed to allow both semi-quantitative and quantitative analyses with good accuracy over a wide range of cell currents. In addition, the 12-bit ADC embedded into the

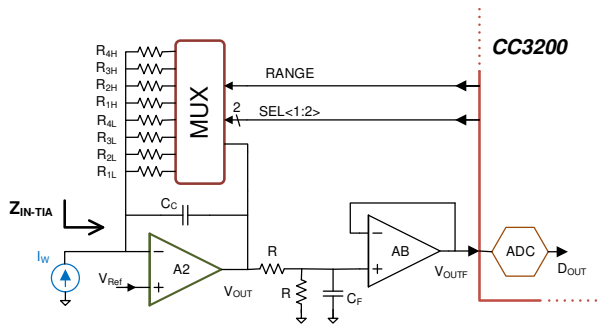

FIGURE 5. TIA with programmable gain.

This article has been accepted for publication in a future issue of this journal, but has not been fully edited. Content may change prior to final publication. Citation information: DOI 10.1109/ACCESS.2021.3120022, IEEE Access

MCU is used for measurement acquisitions, minimizing the component count and simplifying the system design.

A web application with data visualization capability was developed for data visualization and to control the system calibration and configuration. This application was integrated with a cloud service (i.e., MATLAB ThingSpeak [32]) to provide an advanced interface to configure the hardware device and refer to the measurement data. This results in an integrated and flexible platform where different analyses can be defined by setting the parameters of the hardware device. Results can be presented via the web application to the user or to a healthcare professional, who can also access the data history of different users and different analyses, obtaining a complete overview of the users' status. The developed platform does not require the installation of any specific software or app.

In the following sections, the hardware, web application, and cloud services are described in detail.

A. HARDWARE

The potentiostat circuit implemented in the proposed portable device is based on the SEP-2 architecture in Fig. 3(a) [15]. Gain programmability is introduced in the TIA to enable a large reading range of the output current. This aspect is fundamental to ensure a wide measurement range, particularly when the concentration of the biomarker under study ranges over different orders of magnitude. As shown in Fig. 5, the TIA is interfaced to the ADC with a resistive attenuator (6-dB gain-loss) and a buffer. The capacitor C_F is added to limit the bandwidth on the circuit and, thus, the integrated noise. The attenuator limits the maximum ADC input voltage below the absolute maximum rating of 1.8 V [31].

Eight gain levels are obtained by combining a pair of solid-state multiplexers (MUX) with four channels [33]. The enable pin of each MUX allows selecting a set of four resistors (i.e. either R_{1L}-R_{4L} or R_{1H}-R_{4H}), thus obtaining a programmable gain from 10 mV/μA to 1.04 V/μA.

The gain range is selected at the beginning of the measurement procedure. Then, the MCU sets the highest available resistor, i.e. the highest gain, and starts the analysis. Next, the MCU monitors the ADC output during the input signal V_{Sig} sweep. As soon as the converter approaches the output saturation condition, the MCU lowers the TIA gain by changing the SEL<1:2> bus data. Therefore, the potentiostat always works with the maximum possible TIA gain, thus maximizing the Signal-to-Quantization Noise ratio (SQNR) at the ADC input.

However, the variation of the feedback resistance in the TIA is expected to affect the input impedance that, as discussed in the previous section, is a part of the feedback network of the control amplifier, as shown in the circuit schematic of Fig. 6. In the figure, the TIA was replaced with its equivalent input impedance, i.e. $Z_{IN\text{-}TIA} = R_{IN\text{-}TIA} + jX_{IN\text{-}TIA}$. Thus, the stability margin must be evaluated over the range of the TIA gain and the expected range of the faradaic resistance R_{CH} and the equivalent capacitance C_{CH}. In the proposed implementation, the AD8608 [34] is used as the control opamp (A1) and the OPA170 [35] as the TIA opamp.

Finally, an optical barcode scanner (Newland EM3080-W [36]) was introduced and interfaced with the MCU through its UART port. This feature allows the biosensor output to be associated with a particular user through his/her ID card, thus discriminating different tests for different users and building a historical record for each person.

B. CLOUD ANALYTICS AND WEB APPLICATION

Remote configuration and user interaction rely on an integrated web application and MATLAB ThingSpeak cloud service.

The ThingSpeak platform is used as a database for data storage and processing. The storage is achieved by using ThingSpeak Channels and Channel Fields as the equivalent of database tables and tables columns, respectively. For data processing, the MATLAB Analysis and React functionalities of ThingSpeak were exploited. The first one allows MATLAB code to be executed on the cloud to perform analyses on data stored inside Channels, while the latter can be used as a trigger to start the desired MATLAB Analysis script when a condition is met inside a Channel (e.g., a Field is equal to a given value).

The web interface relies on static web pages hosted on a remote server for the frontend and user interaction. The technology used exploits HTML and CSS for the graphical architecture and styling, and JavaScript (along with the jQuery framework) for the functionalities. Moreover, the interface is built on top of the Bootstrap framework, which combines the basic HTML, CSS, and JavaScript elements to provide flexibility to the final application. The application communicates with the cloud platform through the HTTP

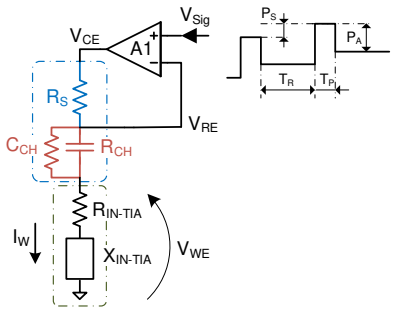

FIGURE 6. CE control amplifier with equivalent load.

This article has been accepted for publication in a future issue of this journal, but has not been fully edited. Content may change prior to final publication. Citation information: DOI 10.1109/ACCESS.2021.3120022, IEEE Access

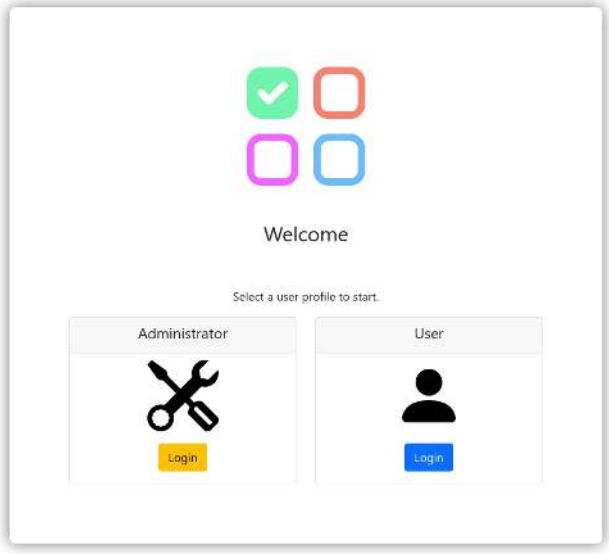

FIGURE 7. **Web application login page.**

REST APIs provided by ThingSpeak, enabling uploading and downloading data from the Channels.

On the first page, the user is asked to select a login mode. As shown in Fig. 7, depending on the operation to perform on the system, one out of two types of profiles can be selected: Administrator or User. These profiles are detailed in the following paragraphs.

1) ADMINISTRATOR PROFILE

The Administrator profile is conceived for the device configuration. New types of analysis can be defined, varying the electrical parameters (i.e. the V_{WE} and V_{RE} voltages applied to the cell), and the associated calibration process as shown in Fig. 8. Once defined, the analysis parameters are sent and stored in the cloud service. In the next operations, they can be reviewed and selected (Fig. 9).

Each set of analyses must be preceded by a calibration process by which a set of parameters characterizing the chosen analytical method, i.e. semi-quantitative or quantitative, are specified (Fig. 10). Generally speaking, if a quantitative analysis is selected, a four parameters logistic regression is required to measure the analyte concentration associated with the analysis. The calibration process can be either manual or automatic. In the first case, a text box allows for manually typing the parameter values. Instead, the automatic calibration is carried out starting from some measurement data corresponding to known concentration values. Once all the necessary measurements have been acquired from the hardware device and uploaded to the cloud service, the selected calibration algorithm can be triggered on the cloud.

Different calibration algorithms can be implemented on the cloud service. Since it is possible to exploit an higher computational power than that of a MCU, even complex algorithms such as those of ML can be performed, obtaining a more powerful and innovative platform. Once the calibration parameters have been computed, they are stored in the

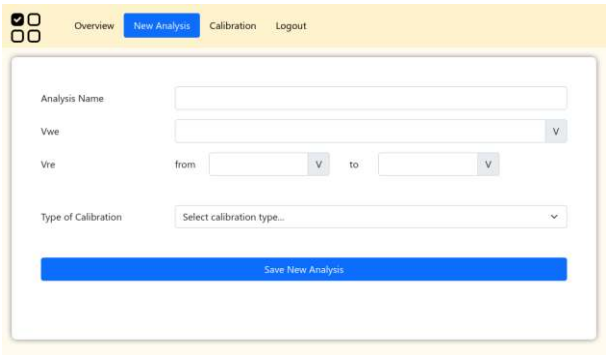

FIGURE 8. **Definition of a new analysis.**

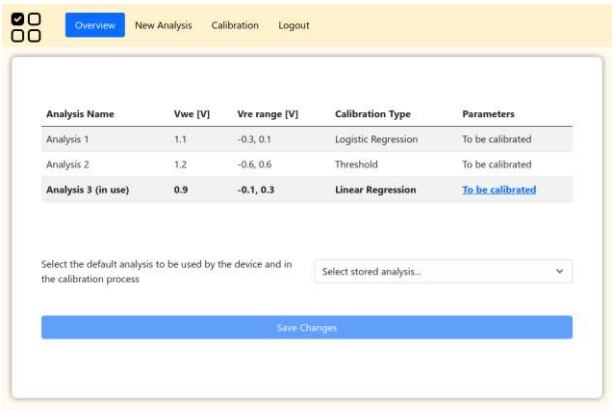

FIGURE 9. **Overview of stored analyses.**

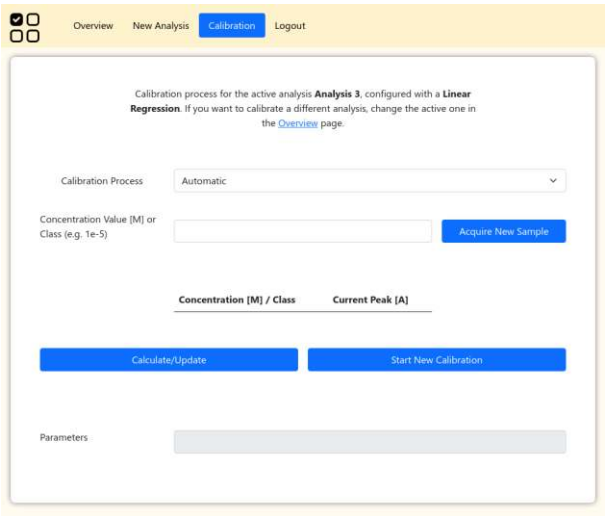

FIGURE 10. **Calibration page.**

database and visualized both in the Parameters field of the calibration page and in the table of the overview page (Fig. 9).

2) USER PROFILE

In the user profile section, the results of the analyses can be reviewed and evaluated. Each time a new test is performed, the hardware device downloads from the cloud the parameters previously computed during the calibration procedure. The user has to insert the screen-printed electrode before starting the acquisition. Moreover, to associate the data with the user, he/she has to scan his/her personal ID number using the

This article has been accepted for publication in a future issue of this journal, but has not been fully edited. Content may change prior to final publication. Citation information: DOI 10.1109/ACCESS.2021.3120022, IEEE Access

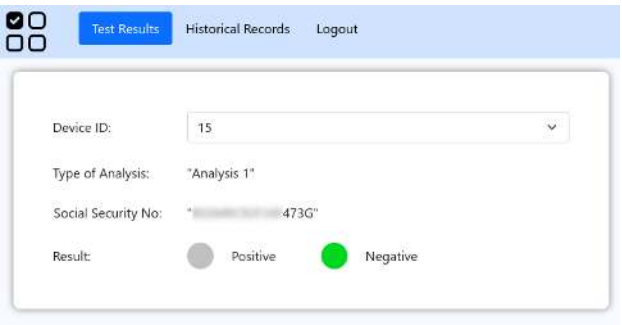

FIGURE 11. User Interface.

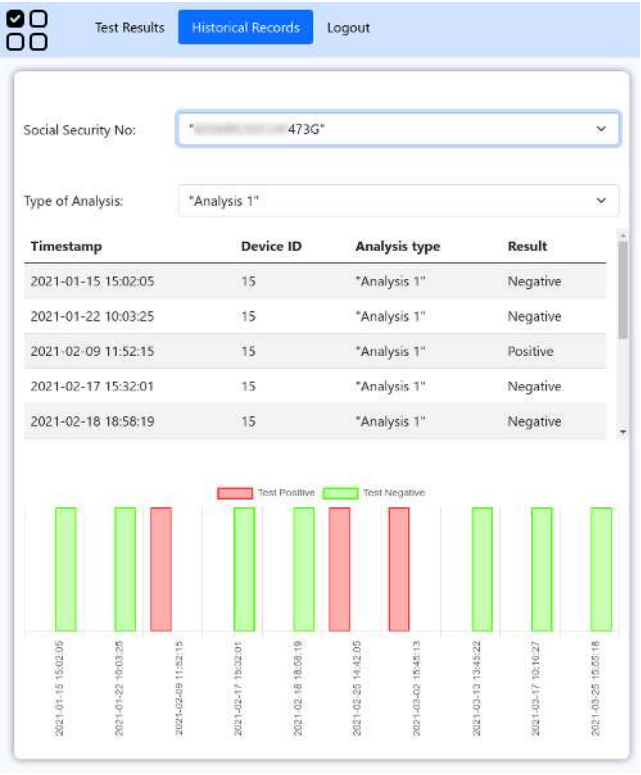

FIGURE 12. Historical records.

barcode scanner. Data processing is carried out on-board thanks to the core section, and results are sent to the cloud for storage and visualization. If a known Wi-Fi connection is not available, the device will store the data into its internal memory: when the connection is restored, the data are uploaded. This choice improves the device power consumption and battery management.

Results can be reviewed by the user on the web page (Fig. 11). Furthermore, thanks to the possibility of pairing each user with his/her tests, a Historical Record can be built (Fig. 12). Here, all the results of a single person can be shown for the user's personal information. In the case of a healthcare professional, the results of different people can be aggregated to give an overview of all the situations of each patient.

III. RESULTS AND DISCUSSION

A. ELECTRICAL CHARACTERIZATION

The electrical Input/Output (I/O) characteristic of the potentiostat in the proposed system was measured using a dummy cell as load [18], [22]. The circuit of this cell corresponds to the electrical model in Fig. 2, without the internal current generator and with R_S=100 Ω and C_{CH}=1μF. Three values of faradaic-equivalent resistance R_{CH} were considered (i.e. 10 kΩ, 100 kΩ, and 1 MΩ), corresponding to the case of a high, intermediate and low output current. All the tests were carried out with V_{Ref} set to 1.2 V and a V_{Sig} span from -0.6 to 0.6 V. In each measurement, the TIA gain was set to the maximum value available in the system but still compatible with the out-of-saturation operation of the ADC in Fig. 5.

Thus, with the lowest, intermediate, and highest value of R_{CH}, the selected TIA feedback resistance is, respectively, 10 kΩ, 102 kΩ, and 1.04 MΩ.

The DC V_{Sig} voltage was externally generated by an accurate Source and Measurement Unit (SMU), whereas the dedicated DAC provided the V_{Ref} reference voltage. The output voltage V_{OUTF} in Fig. 5 was measured with a 6.5 digits voltmeter. The results in Fig. 13 show excellent linearity and R^2 values for the linear fitting that are always close to one over the whole range of faradaic resistance and TIA gain.

The system was also tested with five different concentrations of potassium ferri/ferrocyanide redox probe in aqueous 100 mM KCl as the supporting electrolyte (0.05mM, 0.2mM, 1mM, 2mM, 3mM) to compare the device output with

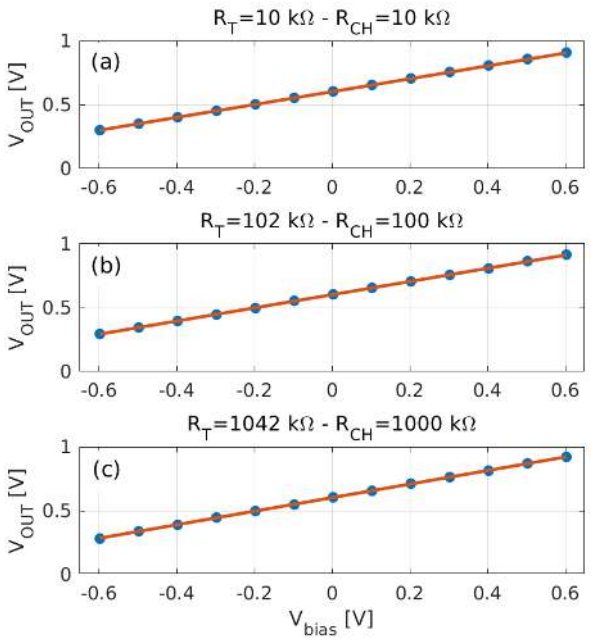

FIGURE 13. Blue circles: Measured potentiostat I/O characteristics with analog input voltage and 10 mV/μA (a), 102 mV/μA (b), and 1.04 V/μA (c) TIA gain. Solid red lines: best-fitting lines.

This article has been accepted for publication in a future issue of this journal, but has not been fully edited. Content may change prior to final publication. Citation information: DOI 10.1109/ACCESS.2021.3120022, IEEE Access

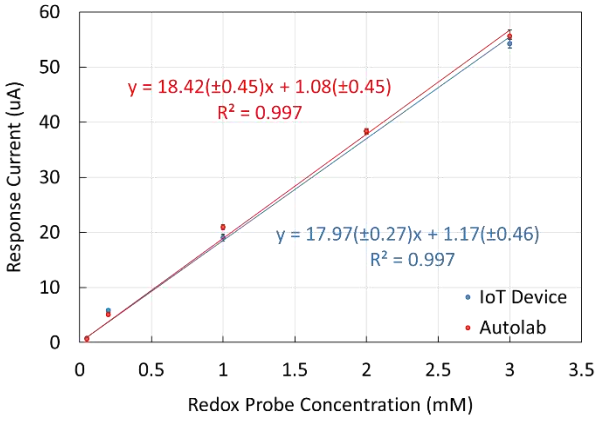

FIGURE 14. Linear regression models for calibration of potassium ferri/ferrocyanide redox probe determined by the portable IoT-based and commercial Autolab potentiostat. Mean values and standard deviation (error bars) are reported in parentheses (*n=3*)

that obtained with a commercial bench-top instrument (Autolab PGSTAT 204). Three replicated acquisitions were carried out for each concentration level with both the bench-top instrument and our smart potentiostat (Fig. 14). The regression functions calculated with the proposed device and the Autolab do not show significantly different slope values ($p>0.05$), thus highlighting no differences in analytical sensitivity. As for goodness of fit, the same value of R^2 was obtained in both cases.

B. APPLICATION-SPECIFIC TESTS: MACHINE LEARNING APPLIED TO SEMI-QUANTITATIVE ANALYSES

Thanks to the features enabled by the cloud service, advanced algorithms can be applied to the calibration of the device. In the case of semi-quantitative analysis, ML approaches can be exploited to train the system and classify the samples according to a predefined rule (e.g. positives, negatives, weak positives, etc.). Different algorithms can be applied to this task and they can be classified according to whether they need labeled input data for training (supervised learning algorithms) or not (unsupervised learning algorithms). Support Vector Machines (SVM) are a class of supervised algorithms that return an optimal decision boundary (i.e., separating hyperplane) dividing input train samples. The data points closest to the hyperplane are known as Support Vectors and are exploited to characterize new input samples in the test phase. The SVM model was proposed in [37], [38]. In the original conceptualization, the SVM algorithm constructs a linear decision boundary that maximizes the separation in two classes of a dataset in the 2-dimensional space. In its generalization [39], the SVM finds a hyperplane that maximizes the separation of the data points into their potential k-classes in an n-dimensional space. Since the data are usually non-linearly distributed, complex data transformations must be performed using appropriate Kernel Functions operating on the training data to transform a non-linear decision surface into a linear equation in a higher number of dimensions space.

In this work, an SVM algorithm has been applied to a semi-quantitative analysis to classify the input samples into four different classes. Usually, in the semi-quantitative analysis, the goal is to discriminate between samples above or below a reference value, i.e., a threshold. The threshold identification is not an easy task, and the SVM can be adopted to classify the acquired data properly.

Four different concentrations (i.e., 0.05, 0.2, 1, and 5mM) levels of potassium ferri/ferrocyanide redox probe in aqueous 100 mM KCl as the supporting electrolyte have been analyzed. Fifty acquisitions have been carried out for each concentration for a total of 200 values acquired. Twenty of them have been selected for the training set, leaving the remaining for the test set. The splitting data process has been repeated 100 times, and for each resulting training set, a linear SVM model was trained. A linear kernel was used since it is the least demanding from a computational power point of view. Since the cloud platform chosen is MATLAB ThingSpeak, MATLAB SVM functions were exploited for this purpose. In particular, the *fitcecoc* function was selected to build the multiclass model. Since this test aims to demonstrate the feasibility of the approach made available by the new smart potentiostat architecture, no hyperparameters optimization was set up at this stage and the default one-versus-one coding design was used. The model was validated with 10-fold cross-validation against the training set. The accuracy was estimated starting from the *kfoldLoss* MATLAB function, returning the loss obtained from the cross-validated classification model. *'ClassifError'* option was selected for the loss function. Then the accuracy of the training set *TrainAcc* was evaluated as:

$$TrainAcc = (1 - \ kfoldLoss) * 100 \qquad (1)$$

An average accuracy of 98.5% was obtained over the 100 train sets generated.

The test set was used to check whether the model correctly classifies even unseen data. The model capability to correctly classify new samples was evaluated with the following accuracy function:

$$TestAcc = 100 - \ (total\ errors)/(total\ of\ data) * 100 \qquad (2)$$

Average classification accuracy of 98.23% was obtained over the 100 considered test sets.

In Fig. 15, the worst-case confusion matrix is shown. Each row of the matrix represents the instances in the true class, while each column represents the instances in the predicted class. The green squares represent the number of the instances correctly classified. The most misclassified classes are those related to 0.05mM and 0.2mM concentration, which exhibit similar current responses. As shown, the results fully confirm the good capability to discriminate each class even in the worst-case scenario. Moreover, this test demonstrates the

This article has been accepted for publication in a future issue of this journal, but has not been fully edited. Content may change prior to final publication. Citation information: DOI 10.1109/ACCESS.2021.3120022, IEEE Access

feasibility of this approach and the advantages that smart potentiostats can achieve with the proposed architecture.

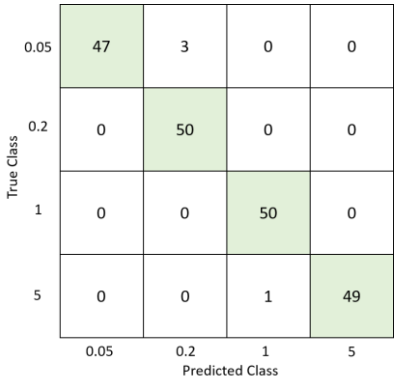

FIGURE 15. Worst-case confusion matrix for 200 ferri/ferrocyanide acquisitions

C. APPLICATION-SPECIFIC TESTS: HYDROQUINONE PROBE APPLIED TO PoC BIOSENSORS FOR COVID-19

Finally, to prove that the device is fully configurable for a different application, an acquisition with hydroquinone (HQ) was carried out. In fact, HQ is the enzyme reaction product of hydroquinone diphosphate (HQDP), i.e, the typical enzyme substrate used for the readout of signals generated by biosensors intended for PoC applications, exploiting alkaline phosphatase (ALP) as enzyme label [19], [20]. For example, specific human antibodies directed against SARS-CoV-2 viral proteins are usually discriminated in terms of IgG or IgM isotypes and detected/quantified in the context of serological tests by means of ALP-labelled anti-human secondary antibodies. The result shown in Fig. 16 proves that the developed portable potentiostat could provide fast data acquisition, exhibiting the potential as a smart PoCT device to reduce the dependence on bulky instrumentation for diagnostic purposes. Efforts are being made to integrate the portable IoT-based device with sensing platforms to allow easy operation and data management for COVID-19 diagnosis.

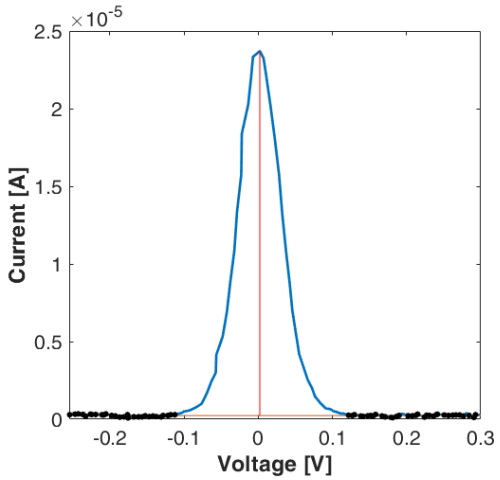

FIGURE 16. DPV response acquired with the smart potentiostat in a 5mM solution of hydroquinone in alkaline buffer (pH=9.8)

IV. CONCLUSION

In this paper, an innovative platform for electrochemical analyses in biosensor applications is presented. The proposed approach relies on a custom hardware designed to be competitive with commercial bench-top instruments, the ThingSpeak cloud service for data storage and analytics, and a custom web application for remote access and control. This smart potentiostat was designed to ensure maximum flexibility and reconfigurability. Excellent linearity was obtained, considering three different faradaic resistance values corresponding to different output current levels. Moreover, by comparing the portable device with a commercial bench-top instrument, a good correlation between the two potentiostats for the ferri/ferrocyanide redox probe was achieved.

The device was also tested in some application examples to demonstrate the advantages of the proposed approach. The feasibility of applying an SVM model to semi-quantitative analyses for the classification among four concentration classes was proved. In addition, the suitability of the smart device for PoC applications for COVID-19 diagnosis was demonstrated.

Future research directions will be aimed at investigating other architectural solutions, especially in the presence of a high number of devices on the same IoT network [40]. Furthermore, it could be interesting to assess the ability to classify the input sample in semi-quantitative analyses in the case of low analytical sensitivity, also investigating the use of ML techniques.

The suitability of the developed system is being tested for the acquisition and processing of data from serological or antigenic diagnostic testing related to SARS-CoV-2 viral infection exploiting the immobilization of specific bioreceptors on disposable screen-printed electrodes. For this purpose, the biosensing devices will be validated in biological fluids of diagnostic concern to assess their sensitivity and specificity.

REFERENCES

[1] V. Sharma, I. You, K. Andersson, F. Palmieri, M. H. Rehmani, and J. Lim, "Security, Privacy and Trust for Smart Mobile- Internet of Things (M-IoT): A Survey," *IEEE Access*, vol. 8, pp. 167123–167163, 2020.

[2] A. Boni, V. Bianchi, A. Ricci, and I. De Munari, "NB-IoT and Wi-Fi Technologies: An Integrated Approach to Enhance Portability of Smart Sensors," *IEEE Access*, vol. 9, pp. 74589–74599, 2021.

[3] M. Pateraki *et al.*, "Chapter 2 - Biosensors and Internet of Things in smart healthcare applications: challenges and opportunities," in *Advances in ubiquitous sensing applications for healthcare*, vol. 7, N. Dey, A. S. Ashour, S. James Fong, and C. B. T.-W. and I. M. D. Bhatt,

Eds. Academic Press, 2020, pp. 25–53.

[4] N. Afsarimanesh, M. E. E. Alahi, S. C. Mukhopadhyay, and M. Kruger, "Development of IoT-Based Impedometric Biosensor for Point-of-Care Monitoring of Bone Loss," *IEEE J. Emerg. Sel. Top. Circuits Syst.*, vol. 8, no. 2, pp. 211–220, 2018.

[5] Y. Yuan *et al.*, "Development of an Internet of Things Based Electrochemical Microfluidic System for Free Calcium Detection," *Applied Sciences* , vol. 8, no. 8. 2018.

[6] J. Smith and V. Hinson-Smith, "Product Review: The Potentiostat: Electrochemistry's Utility Player," *Anal. Chem.*, vol. 74, no. 19, pp. 539 A-541 A, 2002.

[7] A. F. D. Cruz, N. Norena, A. Kaushik, and S. Bhansali, "A low-cost miniaturized potentiostat for point-of-care diagnosis," *Biosens. Bioelectron.*, vol. 62, pp. 249–254, Dec. 2014.

[8] S. Jain *et al.*, "Internet of medical things (IoMT)-integrated biosensors for point-of-care testing of infectious diseases," *Biosens. Bioelectron.*, vol. 179, no. September 2020, p. 113074, 2021.

[9] C. Adrover-Jaume *et al.*, "Paper biosensors for detecting elevated IL-6 levels in blood and respiratory samples from COVID-19 patients," *Sensors Actuators, B Chem.*, vol. 330, no. October 2020, 2021.

[10] Y. Tao, F. Luo, Y. Lin, N. Dong, C. Li, and Z. Lin, "Quantitative gold nanorods based photothermal biosensor for glucose using a thermometer as readout," *Talanta*, vol. 230, no. January, p. 122364, 2021.

[11] A. Radovici, I. Culic, D. Rosner, and F. Oprea, "A model for the remote deployment, update, and safe recovery for commercial sensor-based iot systems," *Sensors (Switzerland)*, vol. 20, no. 16, pp. 1–34, 2020.

[12] S. M. Martin, F. H. Gebara, T. D. Strong, and R. B. Brown, "A low-voltage, chemical sensor interface for systems-on-chip: the fully-differential potentiostat," in *2004 IEEE International Symposium on Circuits and Systems*, 2004, vol. 4, pp. IV-892–895.

[13] R. J. Reay, S. P. Kounaves, and G. T. A. Kovacs, "An integrated CMOS potentiostat for miniaturized electroanalytical instrumentation," in *Proceedings of IEEE International Solid-State Circuits Conference - ISSCC '94*, 1994, pp. 162–163.

[14] E. Lauwers, J. Suls, W. Gumbrecht, D. Maes, G. Gielen, and W. Sansen, "A CMOS multiparameter biochemical microsensor with temperature control and signal interfacing," *IEEE J. Solid-State Circuits*, vol. 36, no. 12, pp. 2030–2038, 2001.

[15] V. Bianchi, A. Boni, S. Fortunati, M. Giannetto, M. Careri, and I. De Munari, "A Wi-Fi Cloud-Based Portable Potentiostat for Electrochemical Biosensors," *IEEE Trans. Instrum. Meas.*, vol. 69, no. 6, pp. 3232–3240, 2020.

[16] "LMP91000 Configurable AFE Potentiostat for Low-Power Chemical Sensing Applications | TI.com." .

[17] K. L. Kraver *et al.*, "A mixed-signal sensor interface microinstrument," *Sensors Actuators A Phys.*, vol. 91, no. 3, pp. 266–277, 2001.

[18] S. D. Adams, E. H. Doeven, K. Quayle, and A. Z. Kouzani, "MiniStat: Development and Evaluation of a Mini-Potentiostat for Electrochemical Measurements," *IEEE Access*, vol. 7, pp. 31903–31912, 2019.

[19] S. M. Rezaul Hasan, "Stability analysis and novel compensation of a CMOS current-feedback potentiostat circuit for electrochemical sensors," *IEEE Sens. J.*, vol. 7, no. 5, pp. 814–824, 2007.

[20] W. S. Wang, W. T. Kuo, H. Y. Huang, and C. H. Luo, "Wide dynamic range CMOS potentiostat for amperometric chemical sensor," *Sensors*, vol. 10, no. 3, pp. 1782–1797, 2010.

[21] J. Mathault, D. Grenier, and A. Miled, "Counter/reference-based potentiostat architecture analysis and comparison," in *2017 15th IEEE International New Circuits and Systems Conference (NEWCAS)*, 2017, pp. 201–204.

[22] J. P. De Campos Da Costa, W. B. Bastos, P. I. Da Costa, M. A. Zaghete, E. Longo, and J. P. Carmo, "Portable Laboratory Platform with Electrochemical Biosensors for Immunodiagnostic of Hepatitis C Virus," *IEEE Sens. J.*, vol. 19, no. 22, pp. 10701–10709, 2019.

[23] P. Irving, R. Cecil, and M. Z. Yates, "MYSTAT: A compact potentiostat/galvanostat for general electrochemistry measurements," *HardwareX*, vol. 9, p. e00163, 2021.

[24] P. Irving, R. Cecil, and M. Z. Yates, "MYSTAT: A compact potentiostat/galvanostat for general electrochemistry measurements," *HardwareX*, vol. 9, p. e00163, 2021.

[25] J. T. C. Barragan and L. T. Kubota, "Minipotentiostat controlled by smartphone on a micropipette: A versatile, portable, agile and accurate tool for electroanalysis," *Electrochim. Acta*, vol. 341, 2020.

[26] A. V. Cordova-Huaman, V. R. Jauja-Ccana, and A. La Rosa-Toro, "Low-cost smartphone-controlled potentiostat based on Arduino for teaching electrochemistry fundamentals and applications," *Heliyon*, vol. 7, no. 2, p. e06259, 2021.

[27] C. Mercer, R. Bennett, P. Conghaile, J. F. Rusling, and D. Leech, "Glucose biosensor based on open-source wireless microfluidic potentiostat," *Sensors Actuators, B Chem.*, vol. 290, no. January, pp. 616–624, 2019.

[28] M. Giannetto, V. Bianchi, S. Gentili, S. Fortunati, I. De Munari, and M. Careri, "An integrated IoT-Wi-Fi board for remote data acquisition and sharing from innovative immunosensors. Case of study: Diagnosis of celiac disease," *Sensors Actuators, B Chem.*, vol. 273, pp. 1395–1403, Nov. 2018.

[29] V. Bianchi, M. Mattarozzi, M. Giannetto, A. Boni, I. De Munari, and M. Careri, "A self-calibrating iot portable electrochemical immunosensor for serum human epididymis protein 4 as a tumor biomarker for ovarian cancer," *Sensors (Switzerland)*, vol. 20, no. 7, 2020.

[30] M. Bassoli *et al.*, "A smart portable potentiostat for Point-of-Care Testing," in proceedings of *Applepies (Applications in Electronics Pervading Industry, Environment and Society) International Conference*, 2021.

[31] "CC3200 SimpleLink Wi-Fi and Internet-of-Things Solution," 2020. [Online]. Available: https://www.ti.com/product/CC3200. [Accessed: 08-Jun-2021].

[32] "Thingspeak Webpage." [Online]. Available: https://www.mathworks.com/products/thingspeak.html. [Accessed: 25-May-2021].

[33] "ADG704 - Low Voltage 4 Ohm, 4-Channel Multiplexer &Beta." Analog Devices, Inc., Norwood, MA, USA, 1999.

[34] A. D. Inc., "Precision, Low Noise, CMOS, Rail-to-Rail, Input/Output Operational Amplifiers." [Online]. Available: https://www.analog.com/media/en/technical-documentation/data-sheets/AD8605_8606_8608.pdf. [Accessed: 16-Jun-2021].

[35] Texas Instruments, "OPA4170-36V, microPower, Rail-to-Rail Output, Quad, General Purpose Op Amp." [Online]. Available:

https://www.ti.com/product/OPA4170. [Accessed: 16-Jun-2021].

[36] Newland, "EM3080-W web page." [Online]. Available: http://www.newlandamerica.com/h-pd-137.html. [Accessed: 03-Jun-2021].

[37] C. Cortes and V. Vapnik, "Support-vector networks," *Mach. Learn.*, vol. 20, pp. 273–297, 1995.

[38] V. Vapnik, *Statistical learning theory*. 1998.

[39] J. Weston and C. Watkins, "Support vector machines for multi-class pattern recognition," in *7th European Symposium On Artificial Neural Networks*, 1999, pp. 219–224.

[40] D. Ermolenko, C. Kilicheva, A. Muthanna, and A. Khakimov, "Internet of Things Services Orchestration Framework Based on Kubernetes and Edge Computing," *Proc. 2021 IEEE Conf. Russ. Young Res. Electr. Electron. Eng. ElConRus 2021*, pp. 12–17, 2021.